Magnetic nanofibers for remotely triggered catalytic activity applied to the degradation of organic pollutants

J.A. Fuentes-García [a,*], B. Sanz [b], R. Mallada [a,c], M.R. Ibarra [a,d], G.F. Goya [a,d]

[a] *Instituto de Nanociencia y Materiales de Aragón (INMA), CSIC-Universidad de Zaragoza, 50018 Zaragoza, Spain*
[b] *nanoScale Biomagnetics S.L, 50197 Zaragoza, Spain*
[c] *Department of Chemical & Environmental Engineering, University of Zaragoza, 50018 Zaragoza, Spain*
[d] *Departamento de Física de la Materia Condensada, Facultad de Ciencias, Universidad de Zaragoza, 50009 Zaragoza, Spain*

HIGHLIGHTS

- We present the design of a new class of multifunctional composite membranes for inductive heating and degradation of organic pollutants activated by external alternating magnetic fields.
- The synthesis route was based in simple sonochemical and electrospinning protocols that allow scaling-up for industrial uses.
- The heating response from the composite membranes was stable against extreme pH and temperature changes, as well as different liquid media, along successive heating catalytic cycles.
- The catalytic efficiency from the obtained multifunctional membranes retained their (>80%) unchanged after several applications to degrade an organic dye (methylene blue).
- The heating and catalytic stability of these membranes allow remote activation by magnetic fields, in those catalytic and degradation applications in dark/inaccessible situations where photocatalytic reactions cannot be applied.

GRAPHICAL ABSTRACT
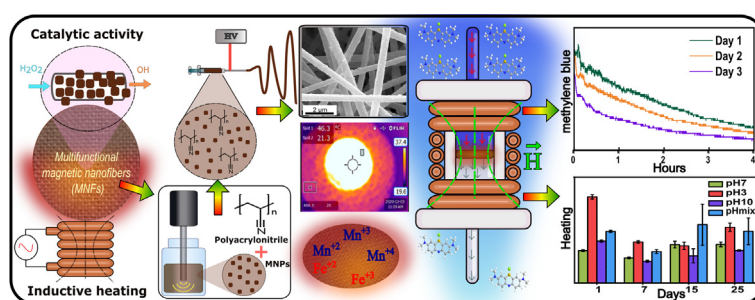
ARTICLE INFO

ABSTRACT

This work reports on the fabrication and characterization of a novel type of electrospun magnetic nanofibers (MNFs), and their application as a magnetically-activable catalysts for degradation of organic pollutants. The magnetic stimulation capability for the catalytic action is provided by iron-manganese oxide ($Mn_xFe_{2-x}O_4$) magnetic nanoparticles (MNPs) embedded into electrospun polyacrylonitrile (PAN), which provides stability and chemical resistance. The MNPs (average size d = 40 ± 7 nm) were first obtained by a green and fast sonochemical route, and subsequently embedded into electrospun PAN nanofibers. The final MNFs showed an average diameter of 760 ± 150 nm, providing a superhydrophobic surface with

* Corresponding author.
   E-mail address: jesus_spirit69@hotmail.com (J.A. Fuentes-García).

contact angle (θ_c = 165°), as well as a considerable amount ($\approx$ 50 % wt.) of embedded MNPs ($Mn_{0.5}Fe_{2.5}O_4$), thermally stable up to temperatures of 330 °C. The catalytic $Fe^{2+/3+}$/$Mn^{2+/3+/4+}$ active centers on the MNPs of MNF's surface could be remotely activated by alternating magnetic fields (AMF) to degrade the methyl blue (MB). Remarkable stability of the MNFs during heating under extreme pH conditions (3 < pH < 10) was observed along several catalytic cycles. The degradation kinetics in presence of hydrogen peroxide showed followed the Langmuir–Hinshelwood model with an average efficiency > 80 %, after several cycles of reusing the same sample without any regeneration process. The capacity of these materials as a catalytic material with magnetic remote activation makes them appealing for those catalytic applications under conditions of darkness or restrained access, where photocatalytic reaction cannot be achieved.

1. Introduction

Water pollution from industrial and domestic activities demands more and more efficient processes and materials for remediation by pollutant degradation. [1–4]. Nanotechnology have provided many options for the design of organic and inorganic materials with multifunctional responses to accomplish this challenging task. [4–6] Nanomaterials with photocatalytic activity (i.e., degrading of pollutants through the UV/visible radiation) have been extensively studied and tested for water treatment. Although the physical photocatalytic mechanisms have proven effective for pollutant degradation, the need of light irradiation hinders its uses in situations when direct light incidence is not available, such as underground pipes or irrigation systems. [7–9].

The uses of magnetic nanoparticles (MNPs) applied to catalysis have been by large related to the recoverability/reusability of the materials through magnetic field capture. [10] However, *magnetically activable catalysts* has been much less studied so far. The idea behind these catalysts is that heterogeneous catalysis can be improved by local stimulation of the active centers by a remote magnetic field, [11–12] thus opening new possibilities for remote and contactless stimulation in those situations where light is not an option. A small number of previous reports on magnetically switched catalysts, primarily applied to biocatalysis, have been theoretically discussed and experimentally tested.[13–14].

Optimizing the magnetic nanoparticles (MNPs) properties to maximize both their heating efficiency through their specific loss power (SLP, i.e., the power losses per unit mass of magnetic material) and their degradation efficiency requires a complex fine-tuning of physicochemical and magnetic properties. Since the SLP depends critically on the particle size and the effective magnetic anisotropy of the resulting MNPs, an efficient way to tune the SLP is to perform a recursive method given by each specific synthesis route. The subtle differences in crystallinity, lattice defects and oxygen vacancies (in ferrites) are very difficult to control at this level of detail. [4–5] For instance, in the case of pure magnetite Fe_3O_4 MNPs, the magnetic anisotropy dictates that the size of the MNPs should be centered at about 20–25 nm, with a narrow size distribution given the homogeneity of the magnetic phase. This requisite is not related with the specific particle size value, but with the fact that at this critical size, magnetite particles are at the transition from multi- to single-domain magnetic structure, [15] and at this region the magnetic domains form closed-flux magnetic domain structure, resembling a vortex-like structure that are demonstrated to be highly efficient for large SLP values.[16–17].

Our optimization for the SLP of the MNFs was therefore chosen for the specific synthesis route used in this work, i.e., the sonochemistry method in aqueous media. This synthesis protocol provides a fast, cheap, and green method that can provide some grams of magnetic material in few minutes of reaction [18–19].

The energy delivered by ultrasound irradiation within aqueous solutions provide the conditions for fast crystallization and controlled growth of nanostructures [20–21]. Given our previous findings showing that soft magnetic materials produced by sonochemistry are better suited for heating by Néel relaxation only,[22] we combined the heating efficiency and catalytic properties in a single material by choosing $Mn_xFe_{2-x}O_4$ MNPs, using the amount × of Mn to tune the magnetic anisotropy for optimal heating. While the softer magnetic phase and specific size provides the heating performance,[23] the Mn/Fe provide the active centers for degradation of organic pollutants. [24].

Composites containing MNPs embedded within a polymeric base material have been successfully used to take advantage from the optical, mechanical, catalytic, and magnetic properties of the active materials adding the stability and durability of the polymer support [25–27]. Embedding MNPs within stable materials provides an efficient strategy to avoid the release of magnetic material into the medium, and to recollect the catalyst for subsequent cycles of degradation in a one-step process [28–29]. In this context, the hybrid magnetic materials can be designed to provide a double purpose: remote inductive heating actuated by magnetic fields [30–33] combined with an inert and flexible support to shape devices for different applications through additive manufacturing techniques [34]. Within this type of manufacturing strategies, polymer-based nanofiber nanomaterials are a common choice for multifunctional approaches both basic research and industrial sectors [35], thanks to its unique capability to be processed using simple procedures for the possibility of add a large variety of optically-, chemically or magnetically-active materials.

Hybrid MNPs-embedded polymer nanofibers can be used for the degradation of organic pollutants from water [36], which can be oxidized and/or degraded by redox catalysis thanks to the presence of transition metal ions onto their surfaces [37]. Transition metal ions are efficient mediators for electron transfer in Fenton-like cyclic reactions [38] in presence of hydrogen peroxide (H_2O_2), producing hydroxyl radicals (OH) and other reactive oxygen species (ROS) that initiate radical polymerization, oxidation, or chlorination reactions [39–40]. For these reactions, pH and temperature have strong influence their efficiency as degradation agents [41].

Electrospinning technique provides a simple and unexpensive option for the fabrication of magnetic nanofibers (MNFs), with potentially scalable to the industrial manufacturing levels [42]. The flexibility of the electrospinning technique to produce a variety of tailored nanofibers relays on the accurate control of the main physical parameters during fabrication, such as the applied voltage or the nozzle-collector working distance, the injection rates, and the viscoelastic properties of the precursor solution [43–44].

In this work, MNFs were designed and obtained for a double purpose, to act as remotely activated nanoheaters [45–46] and as reaction center-points for degradation of heterocyclic organic

tetra-methylthionine chloride dye (methylene blue MB) [47–49], chosen as a proof-of-concept molecule (Fig. 1). The MNFs combine the catalytic capacity of sonochemically produced iron-manganese oxide ($Mn_xFe_{3-x}O_4$) MNPs with the stable and hydrophobic polymer (polyacrylonitrile, PAN) to perform hybrid materials with multifunctional responses.

2. Experimental section

The synthesis route involved simple protocols of materials elaboration and processing towards facile, cost-effective, and scalable manufacturing. Modifying the sonochemical route that we have previously reported for the elaboration of MNPs, a rapid and easy option to produce considerable amounts of MNPs optimized for heating was developed using sulphate salts and reducing the batch-to-batch modifications [22]. After washing and drying, the MNPs were combined with organic solvent to dissolve PAN polymer in a solution prepared for electrospinning. The combination of both electrospinning and sonochemistry to produce hybrid systems represents a promissory route for multifunctional materials using minimal infrastructure.

The chemicals and solvents used in this work were: iron (II) sulphate heptahydrate ($FeSO_4 \cdot 7H_2O$) ReagentPlus® ≥ 99%, manganese (II) sulphate monohydrate ReagentPlus® ≥ 99 % ($MnSO_4 \cdot H_2O$), sodium hydroxide pellets (NaOH) ACS reagent ≥ 97 %, polyacrylonitrile (PAN, $(C_3H_3N)_n$) average Mw 150,000, N,N-dimethylformamide (DMF, $CHON(CH_3)_2$) ReagentPlus® ≥99%, methylene blue hydrated meets analytical specification of BP 73, and hydrogen peroxide solution 34.5–36.5 % were purchased from Merck. Milli-Q deionized water 18.2 MΩ·cm^{-1} was employed in all experiments.

The MNPs were obtained mixing 8:2 ratio of $FeSO_4$ and $MnSO_4$ respectively in 1 L of Milli-Q water for a 5.4 mM solution. After, 90 mL of the prepared Fe^{+2} and Mn^{+2} solution was placed in a 100 mL borosilicate glass bottle (ϕ = 56, h = 100 mm) and the Ti-6A1-4 V 6 mm tip of Ultrasonic Vibra-cell® VCX 130 (20 kHz) equipment was immersed in the center of the reactor. The solution was constantly ultrasonicated at specific energy input 0.27 J/mL during 10 min to reach temperature T ≈ 60 °C. Then, adding 10 mL of NaOH solution (2 N) at 20 mL/min, alkaline conditions for adequate MNPs crystallization were promoted. The reaction is maintained another 10 min under continuous irradiation and after, the ultrasonic processor was turned-off. The resultant solution in the reactor was poured in a beaker with 100 mL of water for lower temperature and pH in the suspension. The described procedure was performed 10 times and the obtained MNP were washed with Milli-Q water using magnetic decantation until pH = 7 in the dispersion. After, we obtain magnetic powder drying MNPs at air atmosphere at 60 °C for three days.

The MNFs precursor solution was elaborated as follows. First, 1 g of MNPs powder was re-dispersed in 10 mL of DMF using ultrasonic bath irradiation for 10 min. The obtained dispersion was placed on magnetic stirring (250 RPM), and heated at 80 °C to improve the solubility of the polymer. Then, 1 g of PAN was dissolved in the DMF-MNPs dispersion with constant stirring for 2 h. Heating was turned-off and stirring continued for 12 h to obtain a homogeneous dispersion of MNPs within the PAN matrix and leading to adequate entanglement of polymeric chains.

Polymeric films composed by MNP@PAN (MNFs samples) were processed injecting 1 mL of the previously prepared precursor solution within the employed electrospinning system which is a laboratory-made version of the classical setup. It consists in a LEGATO® 101 syringe pump (Kd Scientific), used to control the rate injection (0.7 mL/h) of polymer through an AISI 316 stainless steel needle (Oϕ = 1 mm, h = 20 mm). For the applied voltage setup, the positive pole of an adjustable high voltage Power Supply Unit (Genvolt®, 30 W, 200 V − 30 kV) at 8 kV is connected to the needle, while the negative pole was connected to a circular metallic collector (ϕ = 100 mm, h = 30 mm) placed at working distance (distance needle-collector) of 15 cm and covered with aluminum foil. The collected MNFs were trimmed in 10 mm diameter circles for further characterization and evaluation of their inductive heating response and degradation capacity.

2.1. Materials characterization

The characterization methods and the data collected from the experiments can be consulted in "Electrospun magnetic nanofibers for triggered inductive heating and organic pollutants degradation: a characterization dataset" Data in Brief.

2.2. Degradation kinetics of MB under magnetic stimulus

For the characterization of MB degradation under AMF stimulation in continuous mode, the employed setup is described in (Data in Brief, Figure 12) the flow past the modular UV–Vis spectrophotometer allowed for quantitative determination of the dye concen-
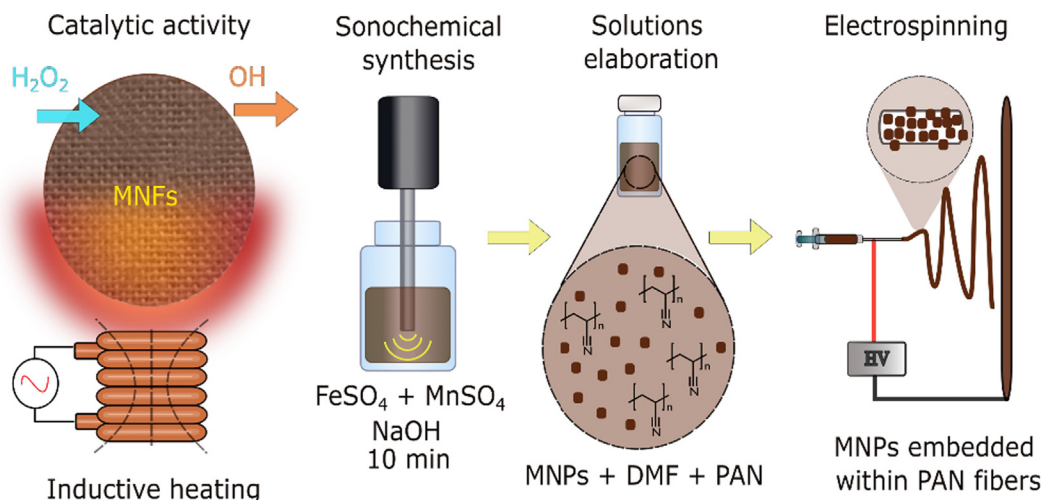

Fig. 1. Schematics of the elaboration strategy for magnetic nanofibers (MNFs) embedded with magnetic nanoparticles (MNPs). Circular membranes composed by stable and hydrophobic polyacrylonitrile combined with magnetic nanoparticles for heating and catalytic applications were intended as separation membrane for water treatment.

tration. A flow rate of 0.4 mL/min was set in a closed-circuit configuration, using a MB solution that flowed through the sample holder containing the MNFs sample (Data in Brief, Figure 12c), placed within the magnetic coil. For these experiments, during the catalytic reaction we selected a target temperature of 35 °C produced by 3 mg of MNFs samples controlled by feedback system to regulate the magnetic field amplitude and stabilize the temperature setpoint during the inductive heating evaluation of the MNFs.

The concentration of MB in real time was measured by a compact modular UV–vis spectrophotometer (USB2000 + VIS-NIR) with halogen light source (HL-2000-FHSA) (Ocean Optics™) bandwidth from 349 to 1019 nm as described in Data in Brief, Figure 12c. The flowing MB solution passed through a PEEK-flow cell with an optical path length of 100 mm and internal volume of 60 μL thus the real time absorbance was monitored. The unavoidable formation of micro-bubbles within the fluing solutions interfered with precise absorbance measurements, and thus a bubble tramp was added before the flow cell to eliminate these effects. The flow cell was optically connected to the spectrophotometer and light source by two optical fibers of 12 mm and 1 m, respectively. All elements were integrated with a software that allowed the control of the many parameters in real time. After systematic analysis and calibration protocols for the UV–vis absorbance experiments, we choose to decrease the signal–noise ratio using a Boxcar Width ($\approx$3200 ms) as integration time and 3 scans to average. MB solutions from 0.08 to 0.8 ppm were flowed to obtain a calibration curve, and the linear fit yielded a final function, y = 2.29 × where y is the absorbance and x = [MB] is the MB concentration.

In all MB degradation experiments, samples were composed by four circular MNFs membranes stacked over each other, providing a total of 3 mg of material, that is the adequate quantity of materials to controls the heating response in the holder, avoiding evaporation and bubble formation. The four samples were supported on a Nylon filter (0.1 μm pore size, ϕ = 13 mm) to retain potential sample debris that could affect the spectrophotometric measurements by crossing the UV–Vis flow cell. Before each experiment a MB solution ([MB] = 0.64 ppm) was circulated during 1.5 h reach adsorption saturation. After this time the MNFs were stimulated turning on the AMF (f = 317.80 kHz; H_0 = 28.3 kA·m^{-1}) in the magnetic applicator to increase the temperature. The MB concentration was monitored continuously in a closed-circuit configuration detecting the 665 nm absorption band and compared with calibration line for the quantification of degraded MB.

3. Results and discussion

3.1. MNFs properties

A large amount (2–5 g) of MNFs has been produced through a fast ($\approx$3h) combination of sonochemical production of the MNPs and subsequent electrospinning of the polymer/MNP mixture. In addition to the low-cost and simplicity, the scalability of both steps in the production is evident: sonochemistry under continuous flow of reactants is already a reality in the industrial sector, with production rates>10 L/min. Also, the industrial sector of electrospun fibers has increased the production rate of dry spinning to a yarn take-up rate of 200–1500 m/min. Improvements such as solventless melt e-spinning adds a greener perspective, which has been proposed as a method for preparing ultrafine fibers with a yield of 10–20 g/h, with a subsequent pilot line of differential e-spinning showing a throughput of 300–600 g/h.[50] These characteristics clearly favor potential translation of our method to the industrial sector.

Regarding the properties of the produced materials, the Scanning Electron Microscopy (SEM) image analysis showed that the resulting fibers were quite homogeneous (Fig. 2 a) with a distribution of fiber diameters with average value ϕ = 760 ± 150 nm, as obtained from the histogram. It was found that the MNPs were successfully embedded in the polymer (Fig. 2 b), Cross section imaging using SEM-FIB dual beam microscopy (Fig. 2 c) revealed that the MNPs were located both on the surface and within the PAN nanofibers. The size of the MNPs (40 ± 7 nm) was consistent with the 38 ± 6 nm previously reported using similar strategy for MNPs synthesis [22].

Optical images of a MNFs membrane (Fig. 2 d) were taken with the sample supported on a Nylon filter (0.1 μm pore size, ϕ = 13 mm) used for the degradation experiments. The brownish color of the MNFs is given by the high concentration of MNPs in the filaments. Further characterization was made employing the same samples geometries as presented in Fig. 2 d as commented bellow.

The Fe and Mn stoichiometry of the MNPs given in atomic percentage (Data in Brief, Fig. 1) showed by EDS analysis was consistent with the spinel ferrite $MnFe_2O_4$ composition. The relationship 80–20 % wt of sulphate precursors ($FeSO_4$ - $MnSO_4$) used during the synthesis resulted in a stoichiometry of $Fe_{2.5}Mn_{0.5}O_4$ (Fe = 83 %, Mn = 17 %) of magnetic material within the MNFs. A minor deficiency of Mn contents was systematically found, as compared with the nominal composition of initial reactants (i.e., $\approx$ 3 % wt. deficiency from the $MnFe_2O_4$ composition). A standard deviation of SD = 1.43 % was obtained from measurements in three different sample areas (Fig. 1 a), indicating that the sonochemical method produced materials with homogeneous composition that can be supported on electrospun nanofibers with reduced composition modification during the elaboration process.

The resulting MNFs showed a superhydrophobic surface, as measured by the water-contact angle (WCA) of θ_C = 165 ° (see Data in Brief, Fig. 2). Previous reports of superhydrophobic properties in PAN nanofibers [51] with contact angles θ_C > 170 ° has been related to the nanostructured aligned nature of the surface and interpreted in terms of the fractional interfacial areas f_1 and f_2 of the nanofibers and the air in the troughs between them. Two key parameters are known to govern the (super)hydrophobic properties: surface energy and roughness, and textured surfaces can diminish surface energy while raising equilibrium contact angles (θc). In rough/textured surfaces the superhydrophobicity can be associated to the existence of a reentrant surface, i.e., in which the surface topography cannot be described by a simple single-valued function f(z) = g(x,y), and a vector projected normal to the x–y plane intersects the surface more than once. Since explained theoretically many years ago, [52] both experiments and theories have confirmed that reentrant surfaces have excellent performance on stabilizing the Cassie state. [53].

This is consistent with the surface topology observed in our nanofibers, where the cross section (see Fig. 2.a) of the samples is composed of cylindrical surfaces randomly stacked. Stacked cylinders form an obvious topology with reentrant surface properties, and this reentrant surface texture is likely to be at the origin of the SHP in our materials. The persistence of the superhydrophobic properties after embedding the MNPs suggests strong chemical interaction between MNPs and the polymer structure, confirmed by the FTIR analysis (Data in Brief, Fig. 3). A strong absorbance in the visible region (380–780 nm) from the MNFs suggest photo-excitability with Eg = 1.75 eV (Data in Brief, Fig. 4). The thermal stability of MNFs was studied through thermogravimetric analysis and differential scanning calorimetry measurements (Data in Brief, Figure 5 and 6). The data showed a glass transition (Tg) expected for the pure PAN fibers at a temperatures Tg = 106 °C (Data in Brief, Figure 5), which shifted to a value of Tg = 112 °C in MNFs samples. This increase of $\approx$ 6 °C is attributed to the incorporation of the MNPs into the PAN matrix and confirmed some degree of interac-
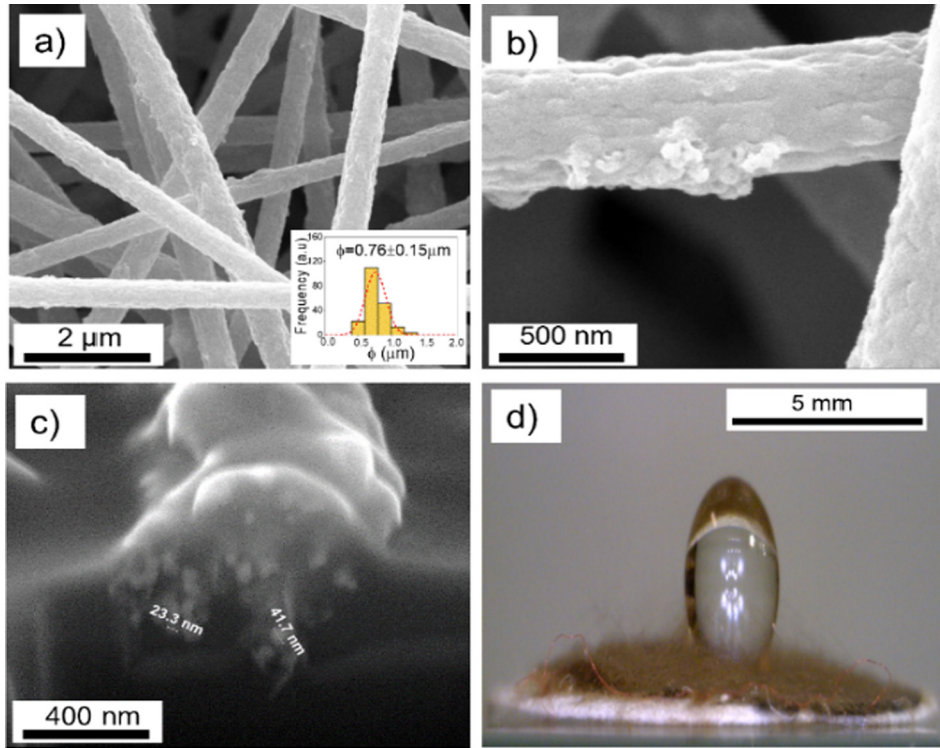
Fig. 2. Scanning electron microscopy images of fabricated magnetic fibers: a) secondary electrons and fiber diameter histogram (inset), b) close-up showing magnetic nanoparticles in the surface, c) cross section of single magnetic fiber, d) optical image of MNFs composed membranes supported on a Nylon filter (ϕ = 13 mm).
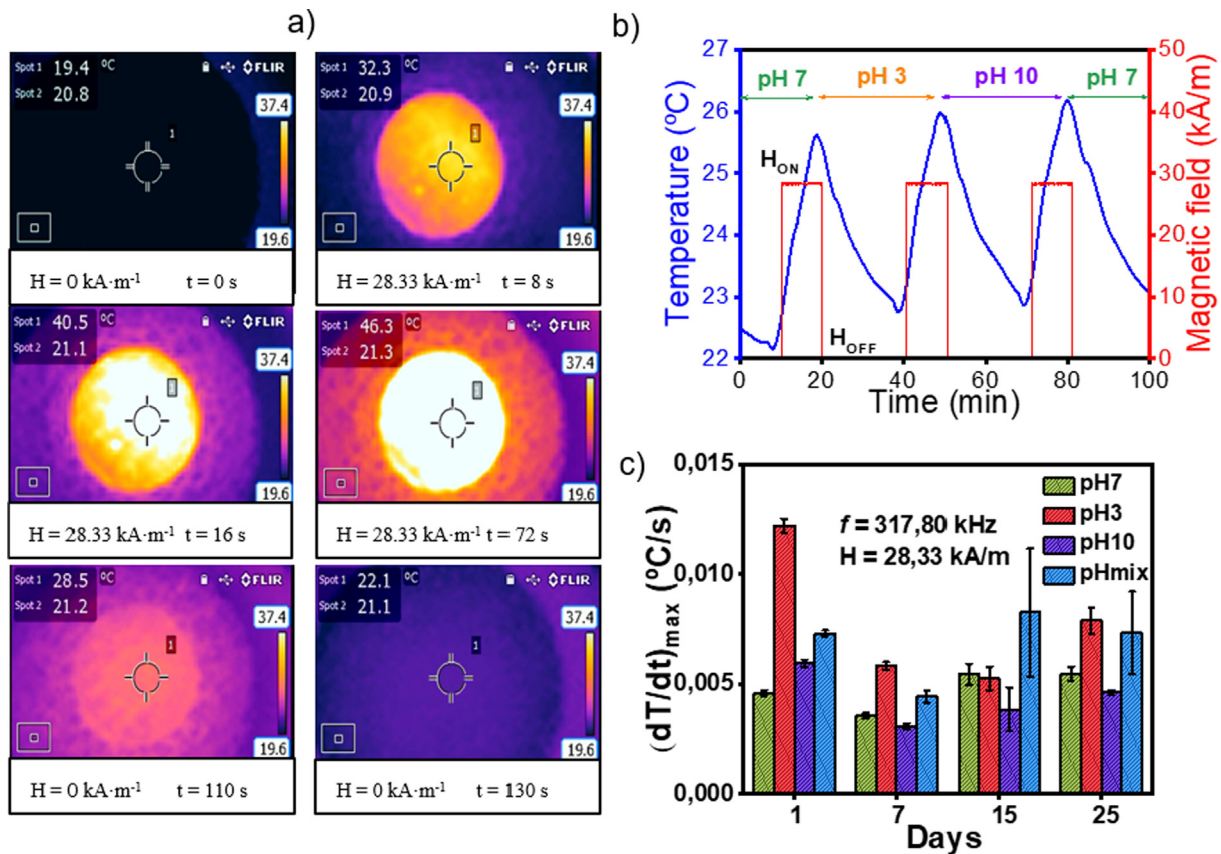

Fig. 3. Heating efficiency performance of MNFs: a) Thermal images corresponding to the fiber placed in the AMF (f = 328 kHz and H = 36.6 kA/m) for 1 min; b) heating capacity of MNFs at dynamic flow conditions applying AMF (317.80 kHz ad 28.33 kA/m) for 10 min. The blue line is temperature (left axe) and the red line the magnetic field applied (right axe), and c) tracking of the heating capacity of fibers with time (f = 317.80 kHz; H_0 = 28.33 kA/m) under aqueous media with different pH values. (For interpretation of the references to color in this figure legend, the reader is referred to the web version of this article.)
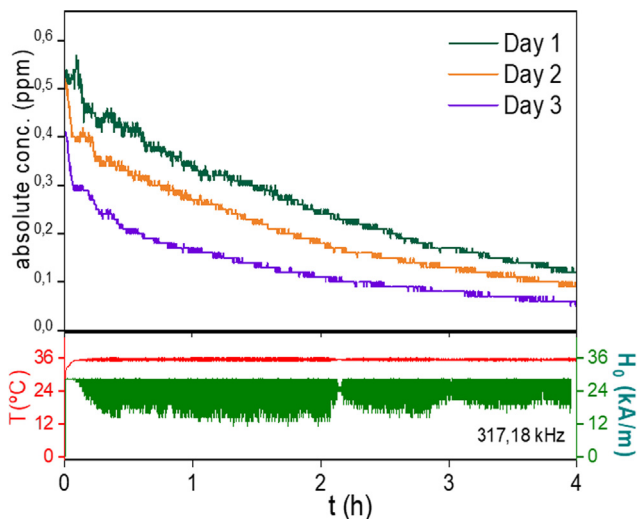
Fig. 4. Upper panel: time dependence data of MB concentration during degradation by MNFs triggered by AMF (H_0 = 24.8 k/m; f = 317,18 kHz), in the presence of H_2O_2 (1.28 ppm) at pH 7. The three curves replicate the experiment re-using the same MNF sample along three different days. Lower panel: registry data for the set point temperature (35 °C, red line) and the changes in H_0 amplitude (green line and right axis) to control the temperature setpoint. The fast changes in H_0 ($\Delta t \approx 5$ s) due to the PI controĺs feedback produces the appearance of a 'thickening' in the H_0 (green) curve. (For interpretation of the references to color in this figure legend, the reader is referred to the web version of this article.)

tion between PAN chains and MNPs, probably due to the interfacial interaction and possible covalent bonding between PAN and the MNPs surface, reducing the mobility of polymer chains [54].

The exothermic transition T ≈ 314 °C in the PAN fibers corresponds to the oligomerization of the nitrile groups within the PAN structure. This transition was not observed in the corresponding thermogram of MNFs, suggesting that the oligomerization of PAN occurs partially with Nitrogen loses and the characteristic transition of nitrile do not occur completely. PAN-sulfur composites have been reported to shift to lower transition temperatures in function of the sulfur contents. The changes in the thermograms can be explained by the interaction of the carbon chains with the sulfur present in the MNPs, that is pyrolyzed at lower temperature 180 °C. These thermal analysis results agreed with FT-IR characterization and together show the structural modification of PAN when is mixed with MNPs for MNFs processing. Both analyses support the idea of a more stable polymer after the spinning process with MNPs, related to the residual sulfate contents from the MNPs synthesis.

Magnetic properties revealed that the saturation magnetization of the composite MNFs (M_S = 15 emu/g at 10 K and M_S = 9 emu·g^{-1} at 300 K) was lowered as compared to the value measured for the MNPs (M_S = 53.5 emu/g) as expected. Taking the M_S (T = 10 K) this value is consistent with a ≈ 28 wt% of MNPs within the fibers. From the M (H) hysteresis loops (Data in Brief, Figure 7) the coercive fields H_C (265 Oe, 10 K and 100 Oe, 300 K) were consistent with the expected values for $MnFe_2O_4$ spinel. The elaborated magnetic materials showed promising Néel relaxation associated inductive heating efficiency under AMF, as revealed the data showed in Figure S8, where the SLP values were evaluated as a function of applied field (12.4 ≤ H_0 ≤ 36.3 kA·m^{-1}, f = 323.75 kHz) for MNPs fixed using gelatin, while MNFs were measured using water as a liquid carrier to temperature sensing from the sample (Data in Brief, Figure 8). The MNFs have remarkable potential as catalysts for water treatment thanks to the presence of Fe^{2+} and Fe^{3+} oxidation states at MNPs surfaces, which are active centers in Fenton-

like reactions and Mn^{2+}, Mn^{3+}, and Mn^{4+} for oxidation of organic compounds in presence of H_2O_2 (Data in Brief, Figure 9).

3.2. Mnfs inductive heating efficiency

The SLP data obtained under different frequencies and fields could be fitted using the allometric expression $SLP(H) = \Phi H^{\lambda}$, with λ = 3.2 and 2.9 for MNPs and MNFs, respectively (Data in Brief, Figure 8). These values of λ differ from the λ = 2 expected for the LRT approximation [55], which is consistent with the relatively large values of H_0 values used in our experiments, that results in a non-linear increase of the M−H hysteresis loop area and therefore a $\lambda > 2$ dependence of the SLP. [56–57].

The obtained SLP values from MNPs samples were larger compared to the MNFs samples under the same AMF conditions. For the maximum field applied, H = 36.3 kA/m, the SLP values were 139.6 ± 6.4 and 83.7 ± 5.5 W/g for MNPs in gelatin and MNFs, respectively, considering the same mass in the samples (3 mg). However, according to the TGA characterization (Data in Brief, Figure 5), about 55% of mass in the MNFs is related to MNPs contents and only the amount of magnetic material in the sample contributes to heating. Assuming a 50% of MNPs contents (discarding 5 % from ashes and residua from non-pyrolyzed polymer) in the MNFs samples, the observed SLP for MNFs is increased (13.8 W/g), if it is compared with the 50% of the value of MNPs samples, suggesting optimized heating efficiency in the MNFs configuration through agglomeration effects or linear arrangements within the fibers, that were reported as an option for increasing the SLP values for magnetic materials [23,58–59].

The heating response of a single MNFs membrane (mass 1 mg) placed in the magnetic applicator system under AMF (f = 328 kHz; H_0 = 36.6 kA/m) was enough to increase the temperature up to 46 °C within the first 60 s (in air) after the field was turned on (Fig. 3 a). These responses and the reached temperature allow to propose the MNFs as local heating agents as for bio applications. The local magnetic heating is known to accelerate the release of drugs and other molecules attached to the samples, and also enhanced crossing through skin barrier has been reported,[60] as well as reducing microorganism population for improved wound healing [61–62]. However, the heating beahaviour can be modified by the environment of the sample and if the media is a liquid carrier.

Subsequently, heating response evaluation using water as liquid carrier, were performed. Response from the MNFs was evaluated at acidic, neutral and alkaline pH conditions. Under these conditions, the membranes were activated using AMF pulses of 10 min and the heating response was recorded (Data in Brief, Figure 10). The heating response from "pH mix" experiment is shown in Fig. 3c. A reproducible heating response was observed for all cycles performed under different pH conditions (pH 7, pH 3, and pH 10) using the same MNFs samples without any reconstruction process. Additionally, we tracked the stability of these response against time by repeating the heating experiments at different pH along 25 days after the first experiment. The resulting values of temperature showing negligible variations within this time lapse.

However, as shown in Fig. 3 c, the evolution of $\frac{dT}{dt\,max}$ has a decreasing tendency compared with the first measurement. This decrement in the rate after the first cycle can be attributed to magnetic materials losses during the experiment. Is possible that the liquid flux carry with the MNPs attached to the surface, besides to the dissolving effect of acid conditions on MNFs. However, after the second cycle the heating response remained stable and the maximum temperature could be reproduced.

The reproducibility of the thermal behaviour of the MNFs can be attributed to the combined thermal stability of the polymer matrix

Table 1

Degradation percentage (η), total mass degraded (m_t), Langmuir - Hinshelwood constants for magnetically activated degradation of MB at T = 35 °C, and goodness-of-fitting according to Nash–Sutcliffe model efficiency (NSE) coefficient criterion.

	η[%]	m_t [µg]	k_r	K	RSME $\cdot 10^{-4}$	SD_{exp}	SD_{model}	NSE
Test 1	81.7	2.4	356.52	0.0028	1.54	0.1105	0.1105	0.9999
Test 2	85	2.5	356.52	0.0028	1.47	0.0928	0.0927	0.9999
Test 3	91.7	2.7	355.58	0.0028	0.87	0.0669	0.0669	0.9999

and the absence of degradation of the MNPs as catalysts. This is consistent with the characterization data (see Section 3.1) that demonstrated that the MNFs structure is thermally stable up to 320 °C. The analysis of the SEM images after the samples were used for the experiments (Data in Brief, Figure 11) confirmed the stability of the morphology of the MNFs.

3.3. MNFs magnetically activated MB degradation

There is a considerable body of experimental and theoretical works on the use of metal and metal oxide nanoparticles on catalytic degradation of organic pollutants in water by enhanced oxidation mechanisms [63]. Those based on iron-containing nanoparticles as active sites for the generation of reactive oxygen species (ROS) have shown remarkable efficacy in the catalytic oxidation of persistent water organic pollutants [64]. However, only some works have reported on the use of magnetic activation to improve or control the catalytic efficacy of magnetic catalysts [65].

Our assessment of MNFs as magnetically activated catalytic membranes was assessed using MB as a target molecule. Before experiment, 5 mL of a solution of 0.64 ppm of MB with H_2O_2 (1.28 µL), was flowed (Q = 0.4 mL/min) for 1.5 h to reach equilibrium and possible adsorption of MB on the MNFs. Once the concentration was stable for several minutes in the UV–Vis module coupled to the magnetic stimulator (Data in Brief, Fig. 1 c), MNFs were remotely stimulated with the AMF (H_0 = 24.8 kA/m; f = 317,18 kHz) and monitored the concentration of MB during 4 h of magnetic field application as presented in Fig. 4.

Fig. 4 shows the gradual decrease in the concentration of MB in the solution within the first at the time window of 4 h of measurements. The control of the target temperature was achieved by using the temperature of the sample as feedback parameter to control the amplitude H_0 of the applied field (Fig. 4, lower panel).

The reusability of the MNFs membranes for MB removal was evaluated three times, one time a day, drying the membranes over night at 60 °C, air atmosphere. For each experiment, initially the MNFs were put in contact at 35 °C with a circulating pure water and kept it for ≈30 min to wet the MNFs. After, the medium was replaced instantly, changing the circulating path (using a zero-dead volume switch valve) from water to the MB solution.

The catalytic activity of MNFs was measured monitoring MB decreasing concentration over the time. The measured degradation time dependence (Fig. 4) shown good agreement with the Langmuir–Hinshelwood (LH) model [66–69], originally developed for heterogeneous photocatalysis through the expression [70]:

$$\frac{1}{r} = \frac{1}{k_r} + \frac{1}{k_r \cdot K \cdot C} \tag{1}$$

where r is the rate of the reaction that changes with time, k_r is the limiting rate constant of reaction, K is the equilibrium constant for adsorption of the substrate onto catalyst and C is the concentration at any time. This model includes the reversible binding of substrate molecules with a multiplicity of active sites at the nanoparticle surface, assuming fast adsorption mechanisms that provides equilibrium at all times [71–72]. The LH modeĺs goodness of the fit to the experimental data was evaluated using the Nash–Sutcliffe model efficiency (NSE) coefficient criterion as hypothesis

testing indicator, using root mean square error (RMSE) and standard deviation (SD) as follows $NSE = 1 - \left(\frac{RSME}{SD}\right)^2$. This coefficient of efficiency of mathematical predictions has a perfect fit at NSE = 1 [73]. Table1 summarizes the kinetics parameters such as degradation percentage (η), using the relation $\eta = \frac{[MB]_0 - [MB]}{[MB]_0} \times 100$, total mass degraded ($m_t$) and the LH degradation kinetics constants k_r and K, and goodness-of-fitting according to NSE.

The obtained value of $\eta > 80\%$ from the first cycle of usage showed the efficiency of MNFs as degradation agent activated by AMF with essentially no decrement on the MB removal capacity after three experiments. Also, the degraded mass was similar after each cycle, showing the reusability of the MNFs as degradation agent. Calculated values of k_r and K were the same in the three cases, this behavior can be associated to stable values for adsorption equilibrium and limiting rates. We can stablish those values as characteristic from the catalytic activity of MNPs embedded in nanofibers of PAN, reported for first time in this work, thanks to the goodness-of-fitting (NSE = 0.9999). As observed in Table 1, the adjusting output shown reduced SD values and quite similar between SD_{exp} and SD_{model}, ensuring that the experimental data are well described by the LH heterogeneous catalysis kinetics.

These results were consistent with a previous work [73] where adsorptions and discoloration of MB was negligible at all temperatures tested due to the MB surface was protonated, except at pH 10 when adsorption was clearly detected. When compared to the works reported by Muñoz et al. [28], our experimental conditions imply a better degradation efficiency since lower concentrations of H_2O_2 and lower temperatures were required in our work to obtain similar catalytic activity on MB.

The observed MB degradation kinetics using MNFs and the degradation response magnetically triggered can be consider as promising result for the application of magnetic materials as water remediation agents. The obtained $\eta > 80\%$ after each cycle of degradation can be attributed to the superhydrophobic behaviour of MNFs ensuring minimal interaction with water soluble molecules, reducing the adsorption and the needs of regeneration procedures for the reusability of the MNFs. Our data can be considered as a proof-of-concept of the possibility of magnetic activation of catalytic membranes for degradation, using materials with the potential to be scaled-up to domestic or industrial applications aiming the treatment of waste water.

4. Conclusions

A simple methodology for the synthesis of hybrid nanomaterials based in polymeric nanofibers and magnetic nanoparticles can be applied to obtain a multifunctional catalyst. This strategy could be easily extended to different polymers and nanoparticles thanks to the versatility of the synthesis rout described here. The MNFs based on hydrophobic PAN polymer provides a reusable degradation catalyst easy to recover after its application, and a sustainable strategy for decontamination at large scales. The composite showed chemical stability against acidic and basic media, while its response to alternating magnetic fields provided a way to remotely switch the catalytic activity on and off thus controlling the redox mechanisms. The degradation kinetics for MB could be

explained in terms of a Langmuir-Hinshelwood mechanism for heterogeneous catalysis, in which the degradation rate is limited by the reaction constant with a slight contribution of the adsorption of molecules on the active sites, with some features resembling allosteric enzymatic activity. Overall, these results showed the potential of MNFs and hydrophobic membranes as catalytic agents for pollutant removal from running water, e.g., underground pipelines with limited access. The employed simple protocols, based in sonochemistry and electrospinning, open the possibility towards scale-up elaboration of materials for industrial applications using basic infrastructure, low toxic precursors and reduced time for the elaboration. Although this work demonstrated the working principle on these materials, further optimization of the degradation efficiency and cost-effectiveness evaluation will be needed for environmental applications such as biological wastes or microplastic degradation.

Data availability

Data is available in Electrospun magnetic nanofibers for triggered inductive heating and organic pollutants degradation: a characterization dataset,http://dx.https://doi.org/10.17632/gt8c5893c4.1.

Declaration of Competing Interest

The authors declare that they have no known competing financial interests or personal relationships that could have appeared to influence the work reported in this paper.

Acknowledgments

Appendix A. Supplementary data

Supplementary data to this article can be found online at https://doi.org/10.1016/j.matdes.2023.111615.

References

[1] A.H. Khan, N.A. Khan, S. Ahmed, A. Dhingra, C.P. Singh, S.U. Khan, A.A. Mohammadi, F. Changani, M. Yousefi, S. Alam, Application of advanced oxidation processes followed by different treatment technologies for hospital wastewater treatment, J. Clean. Prod. 269 (2020), https://doi.org/10.1016/j.jclepro.2020.122411 122411.

[2] A. Sonune, R. Ghate, Developments in wastewater treatment methods, Desalination 167 (2004) 55–63, https://doi.org/10.1016/j.desal.2004.06.113.

[3] G. Crini, E. Lichtfouse, Advantages and disadvantages of techniques used for wastewater treatment, Environ. Chem. Lett. 17 (1) (2019) 145–155, https://doi.org/10.1007/s10311-018-0785-9.

[4] M. Salgot, M. Folch, Wastewater treatment and water reuse, Curr. Opin. Environ. Sci. Health. 2 (2018) 64–74, https://doi.org/10.1016/j.coesh.2018.03.005.

[5] K. Jain, A.S. Patel, V.P. Pardhi, S.J.S. Flora, Nanotechnology in wastewater management: a new paradigm towards wastewater treatment, Molecules. 26 (6) (2021) 1797, https://doi.org/10.3390/molecules26061797.

[6] D. Jassby, T.Y. Cath, H. Buisson, The role of nanotechnology in industrial water treatment, Nature Nanotech. 13 (8) (2018) 670–672, https://doi.org/10.1038/s41565-018-0234-8.

[7] G. Ren, H. Han, Y. Wang, S. Liu, J. Zhao, X. Meng, Z. Li, Recent advances of photocatalytic application in water treatment: a review, Nanomaterials. 11 (7) (2021) 1804, https://doi.org/10.3390/nano11071804).

[8] D. Wang, M.A. Mueses, J.A.C. Márquez, F. Machuca-Martínez, I. Grčić, R.P.M. Moreira, G.L. Puma, Engineering and modeling perspectives on photocatalytic

reactors for water treatment, Water Res. 202 (2021), https://doi.org/10.1016/j.watres.2021.117421 117421.

[9] A.M. Nasir, N. Awang, J. Jaafar, A.F. Ismail, M.H.D. Othman, M.A. Rahman, F. Aziz, M.A.M. Yajid, Recent progress on fabrication and application of electrospun nanofibrous photocatalytic membranes for wastewater treatment: A review, J. Water Process. Eng. 40 (2021), https://doi.org/10.1016/j.jwpe.2020.101878 101878.

[10] V. Polshettiwar, R. Luque, A. Fihri, H. Zhu, M. Bouhrara, J.M. Basset, Magnetically recoverable nanocatalysts, Chem. Rev. 111 (5) (2011) 3036–3075, https://doi.org/10.1021/cr100230z.

[11] L.M. Martínez-Prieto, J. Marbaix, J.M. Asensio, C. Cerezo-Navarrete, P.F. Fazzini, K. Soulantica, B. Chaudret, A. Corma, Ultrastable magnetic nanoparticles encapsulated in carbon for magnetically induced catalysis, ACS Appl. Nano Mater. 3 (7) (2020) 7076–7087, https://doi.org/10.1021/acsanm.0c01392.

[12] H. Mao, Q. Zhang, F. Cheng, Z. Feng, Y. Hua, S. Zuo, A. Cui, C. Yao, Magnetically separable mesoporous Fe$_3$O$_4$@g-C$_3$N$_4$ as a multifunctional material for metallic ion adsorption, oil removal from the aqueous phase, photocatalysis, and efficient synergistic photoactivated fenton reaction, Ind. Eng. Chem. Res. 61 (25) (2022) 8895–8907, https://doi.org/10.1021/acs.iecr.2c01304.

[13] J. Marbaix, N. Mille, L.M. Lacroix, J.M. Asensio, P.F. Fazzini, K. Soulantica, J. Carrey, B. Chaudret, Tuning the composition of FeCo nanoparticle heating agents for magnetically induced catalysis, ACS Appl. Nano Mater. 3 (4) (2020) 3767–3778, https://doi.org/10.1021/acsanm.0c00444.

[14] G.F. Goya, A. Mayoral, E. Winkler, R. Zysler, C. Bagnato, M. Raineri, J.A. Fuentes-García, E. Lima Jr., Next generation of nanozymes: A perspective of the challenges to match biological performance, J. Appl. Phys. 130 (19) (2021), https://doi.org/10.1063/5.0061499 190903.

[15] M.A. Vergés, R. Costo, A.G. Roca, J.F. Marco, G.F. Goya, C.J. Serna, M.d.P. Morales. Uniform and water stable magnetite nanoparticles with diameters around the monodomain–multidomain limit. J. Phys. D: Appl. Phys. 41 (2008) 134003. 10.1088/0022-3727/41/13/134003.

[16] T.P. Almeida, A.R. Muxworthy, A. Kovács, W. Williams, P.D. Brown, R.E. Dunin-Borkowski, Direct visualization of the thermomagnetic behavior of pseudo–single-domain magnetite particles, Science advances 2 (4) (2016) e1501801.

[17] N. Usov, M. Nesmeyanov, V. Tarasov, Magnetic vortices as efficient nano heaters in magnetic nanoparticle hyperthermia, Sci Rep. 8 (2018) 1224, https://doi.org/10.1038/s41598-017-18162-8.

[18] S. Barcikowski, A. Plech, K.S. Suslick, A. Vogel, Materials synthesis in a bubble, MRS Bull. 44 (5) (2019) 382–391, https://doi.org/10.1557/mrs.2019.107.

[19] R. Kumar, V.B. Kumar, A. Gedanken, Sonochemical synthesis of carbon dots, mechanism, effect of parameters, and catalytic, energy, biomedical and tissue engineering applications, Ultrason. Sonochem. 64 (2020), https://doi.org/10.1016/j.ultsonch.2020.105009 105009.

[20] R.J. Wood, J. Lee, M.J. Bussemaker, A parametric review of sonochemistry: Control and augmentation of sonochemical activity in aqueous solutions, Ultrason. Sonochem. 38 (2017) 351–370, https://doi.org/10.1016/j.ultsonch.2017.03.030.

[21] H. Xu, B.W. Zeiger, K.S. Suslick, Sonochemical synthesis of nanomaterials, Chem. Soc. Rev. 42 (7) (2013) 2555–2567, https://doi.org/10.1039/C2CS35282F.

[22] J.A. Fuentes-García, A.C. Alavarse, A.C. Moreno Maldonado, A. Toro-Córdova, M.R. Ibarra, G.F. Goya. Simple sonochemical method to optimize the heating efficiency of magnetic nanoparticles for magnetic fluid hyperthermia. ACS Omega. 5 (41) (2020) 26357-26364. 10.1021/acsomega.0c02212.

[23] D.P. Valdés, E. Lima, R.D. Zysler, G.F. Goya, E. De Biasi, Role of anisotropy, frequency, and interactions in magnetic hyperthermia applications: Noninteracting nanoparticles and linear chain arrangements, Phys. Rev. Applied 15 (2021), https://doi.org/10.1103/PhysRevApplied.15.044005 044005.

[24] Q. Li, X. Jiang, Y. Lian, The efficient photocatalytic degradation of organic pollutants on the MnFe$_2$O$_4$/BGA composite under visible light, Nanomaterials. 11 (5) (2021) 1276, https://doi.org/10.3390/nano11051276.

[25] M. Zhang, W. Song, Y. Tang, X. Xu, Y. Huang, D. Yu, Polymer-based nanofiber-nanoparticle hybrids and their medical applications, Polymers. 14 (2) (2022) 351, https://doi.org/10.3390/polym14020351.

[26] W. Park, H. Shin, B. Choi, W.-K. Rhim, K. Na, D.K. Han, Advanced hybrid nanomaterials for biomedical applications, Prog. Mater. Sci. 114 (2020), https://doi.org/10.1016/j.pmatsci.2020.100686 100686.

[27] T. Pirzada, Z. Ashrafi, W. Xie, S.A. Khan, Cellulose silica hybrid nanofiber aerogels: from sol-gel electrospun nanofibers to multifunctional aerogels, Adv. Funct. Mater. 30 (5) (2020) 1907359, https://doi.org/10.1002/adfm.201907359.

[28] M. Muñoz, J. Nieto-Sandoval, E. Serrano, Z.M. de Pedro, J.A. Casas, CWPO intensification by induction heating using magnetite as catalyst, J. Environ. Chem. Eng. 8 (5) (2020), https://doi.org/10.1016/j.jece.2020.104085 104085.

[29] A. Gallo-Cordova, S. Veintemillas-Verdaguer, P. Tartaj, E. Mazarío, M.d.P. Morales, J.G. Ovejero. Engineering iron oxide nanocatalysts by a microwave-assisted polyol method for the magnetically induced degradation of organic pollutants. Nanomaterials. 11 (4) (2021) 1052. 10.3390/nano11041052.

[30] X. Chen, L. Cheng, H. Li, A. Barhoum, Y. Zhang, X. He, W. Yang, M.M. Bubakir H., Chen. Magnetic nanofibers: unique properties, fabrication techniques, and emerging applications. ChemistrySelect. 3 (31) (2018) 9127-9143. 10.1002/slct.201702480.

[31] C. Döpke, T. Grothe, P. Steblinski, M. Klöcker, L. Sabantina, D. Kosmalska, T. Blachowicz, A. Ehrmann, Magnetic nanofiber mats for data storage and

transfer, Nanomaterials. 9 (1) (2019) 92, https://doi.org/10.3390/nano9010092.

[32] T. Blachowicz, A. Ehrmann. Most recent developments in electrospun magnetic nanofibers: A review. J. Eng. Fibers Fabr. 15 (2020) 1558925019900843. 10.1177/1558925019900843.

[33] M. Radmansouri, E. Bahmani, E. Sarikhani, K. Rahmani, F. Sharifianjazi, M. Irani, Doxorubicin hydrochloride-loaded electrospun chitosan/cobalt ferrite/titanium oxide nanofibers for hyperthermic tumor cell treatment and controlled drug release, Int. J. Biol. Macromol. 116 (2018) 378–384, https://doi.org/10.1016/j.ijbiomac.2018.04.161.

[34] O. Laguna, P. Lietor, F.I. Godino, F. Corpas-Iglesias, A review on additive manufacturing and materials for catalytic applications: Milestones, key concepts, advances and perspectives, Mater. Des. 208 (2021), https://doi.org/10.1016/j.matdes.2021.109927 109927.

[35] I. Alghoraibi, S. Alomari. Different methods for nanofiber design and fabrication, in: A. Barhoum, M. Bechelany, A.S.H. Makhlouf (Eds.), Handbook of nanofibers, Springer, 2019, 1–46.

[36] M. Yanilmaz, M. Dirican, A.M. Asiri, X. Zhang, Flexible polyaniline-carbon nanofiber supercapacitor electrodes, J Energy Storage. 24 (2019) https://doi.org/10.1016/j.est.2019.100766 100766.

[37] A. Romano, I. Ortiz, A.M. Urtiaga, Comprehensive kinetics of electrochemically assisted ammonia removal in marine aquaculture recirculating systems, J. Electroanal. Chem. 897 (2021), https://doi.org/10.1016/j.jelechem.2021.115619 115619.

[38] E.T. Denisov, O.M. Sarkisov, G.I. Likhtenshtein, Chapter 16 - Redox catalysis, in: E.T. Denisov, O.M. Sarkisov, G.I. Likhtenshtein (Eds.), Chemical kinetics, Amsterdam, Elsevier Science, 2003, pp. 452–471.

[39] R. Francke, R.D. Little, Redox catalysis in organic electrosynthesis: basic principles and recent developments, Chem. Soc. Rev. 43 (8) (2014) 2492–2521, https://doi.org/10.1039/C3CS60464K.

[40] J.P. Kehrer, The Haber-Weiss reaction and mechanisms of toxicity, Toxicology. 149 (1) (2000) 43–50, https://doi.org/10.1016/s0300-483x(00)00231-6.

[41] L. Zhang, C. Song, J. Zhang, H. Wang, D.P. Wilkinson, Temperature and pH dependence of oxygen reduction catalyzed by iron fluoroporphyrin adsorbed on a graphite electrode, J. Electrochem. Soc. 152 (12) (2005) A2421, https://doi.org/10.1149/1.2109667.

[42] R.A. Surmenev, A.N. Ivanov, A. Cecilia, T. Baumbach, R.V. Chernozem, S. Mathur, M.A. Surmeneva, Electrospun composites of poly-3-hydroxybutyrate reinforced with conductive fillers for in vivo bone regeneration, Open Ceramics. 9 (2022), https://doi.org/10.1016/j.oceram.2022.100237 100237.

[43] A. Haider, S. Haider, I.K. Kang, A comprehensive review summarizing the effect of electrospinning parameters and potential applications of nanofibers in biomedical and biotechnology, Arab. J. Chem. 11 (8) (2018) 1165–1188, https://doi.org/10.1016/j.arabjc.2015.11.015.

[44] H. M.; Ibrahim, Klingner, A., A review on electrospun polymeric nanofibers: Production parameters and potential applications. Polym. Test. 90 (2020) 106647. 10.1016/j.polymertesting.2020.106647.

[45] J.A. Fuentes-García, A.C. Alavarse, C.E. de Castro, F.C. Giacomelli, M.R. Ibarra, J.J. Bonvent, G.F. Goya, Sonochemical route for mesoporous silica-coated magnetic nanoparticles towards pH-triggered drug delivery system, J. Mater. Res. Technol. 15 (2021) 52–67, https://doi.org/10.1016/j.jmrt.2021.08.014.

[46] N. Zufelato, V.R.R. Aquino, N. Shrivastava, S. Mendanha, R. Miotto, A.F. Bakuzis, Heat generation in magnetic hyperthermia by manganese ferrite-based nanoparticles arises from Néel collective magnetic relaxation, ACS Appl. Nano Mater. 5 (5) (2022) 7521–7539, https://doi.org/10.1021/acsanm.2c01536.

[47] M. Li, Q. Gao, T. Wang, Y.S. Gong, B. Han, K.S. Xia, C.G. Zhou, Solvothermal synthesis of $Mn_xFe_{3-x}O_4$ nanoparticles with interesting physicochemical characteristics and good catalytic degradation activity, Mater. Des. 97 (2016) 341–348, https://doi.org/10.1016/j.matdes.2016.02.103.

[48] Z. Liu, Z. Gao, Q. Wu, Activation of persulfate by magnetic zirconium-doped manganese ferrite for efficient degradation of tetracycline, Chem. Eng. J. 423 (2021), https://doi.org/10.1016/j.cej.2021.130283 130283.

[49] A. Almahri, The solid-state synthetic performance of bentonite stacked manganese ferrite nanoparticles: adsorption and photo-fenton degradation of MB dye and antibacterial applications, J. Mater. Res. Technol. 17 (2022) 2935–2949, https://doi.org/10.1016/j.jmrt.2022.02.052.

[50] C. Mingjun, Z. Youchen, L. Haoyi, L. Xiangnan, D. Yumei, M.M. Bubakir, Y. Weimin, An example of industrialization of melt electrospinning: Polymer melt differential electrospinning, Adv. Ind. Eng. Polym. Res. 2 (3) (2019) 110–115, https://doi.org/10.1016/j.aiepr.2019.06.002.

[51] L. Feng, S. Li, H. Li, J. Zhai, Y. Song, L. Jiang, D. Zhu, Super-hydrophobic surface of aligned polyacrylonitrile nanofibers, Angew. Chem. Int. Ed. 41 (7) (2002) 1221–1223, https://doi.org/10.1002/1521-3773(20020402)41:7<1221::AID-ANIE1221>3.0.CO;2-G.

[52] N.A. Patankar, Hydrophobicity of surfaces with cavities: making hydrophobic substrates from hydrophilic materials?, J Adhes. Sci. Technol. 23 (3) (2009) 413–433, https://doi.org/10.1163/156856108X370073.

[53] H. Shams, K. Basit, M.A. Khan, S. Saleem, A. Mansoor, Realizing surface amphiphobicity using 3D printing techniques: A critical move towards manufacturing low-cost reentrant geometries, Addit. Manuf. 38 (2021), https://doi.org/10.1016/j.addma.2020.101777 101777.

[54] Z. Song, X. Hou, L. Zhang, S. Wu, Enhancing crystallinity and orientation by hot-stretching to improve the mechanical properties of electrospun partially aligned polyacrylonitrile (PAN) nanocomposites, Materials. 4 (4) (2011) 621–632, https://doi.org/10.3390/ma4040621.

[55] N. Usov, B.Y. Liubimov, Dynamics of magnetic nanoparticle in a viscous liquid: Application to magnetic nanoparticle hyperthermia, J. Appl. Phys. 112 (2) (2012), https://doi.org/10.1063/1.4737126 023901.

[56] B. Sanz, M.P. Calatayud, E. De Biasi, E. Lima, M.V. Mansilla, R.D. Zysler, M.R. Ibarra, G.F. Goya, In silico before in vivo: how to predict the heating efficiency of magnetic nanoparticles within the intracellular space, Sci. Rep. 6 (2016) 38733, https://doi.org/10.1038/srep38733.

[57] L. León Félix, B. Sanz, V. Sebastián, T. Torres, M.H. Sousa, J. Coaquira, M.R. Ibarra, G.F. Goya, Gold-decorated magnetic nanoparticles design for hyperthermia applications and as a potential platform for their surface-functionalization, Sci. Rep. 9 (2019) 4185, https://doi.org/10.1038/s41598-019-40769-2.

[58] A.Y. Zubarev, Effect of internal chain-like structures on magnetic hyperthermia in non-liquid media, Philos. Trans. Royal Soc. A. 377 (2143) (2019) 20180213, https://doi.org/10.1098/rsta.2018.0213.

[59] M. Molcan, K. Kaczmarek, M. Kubovcikova, H. Gojzewski, J. Kovac, M. Timko, A. Józefczak, Magnetic hyperthermia study of magnetosome chain systems in tissue-mimicking phantom, J. Mol. Liq. 320 (2020), https://doi.org/10.1016/j.molliq.2020.114470 114470.

[60] S. Szunerits, R. Boukherroub, Heat: a highly efficient skin enhancer for transdermal drug delivery, Front. Bioeng. Biotechnol. 6 (2018) 15, https://doi.org/10.3389/fbioe.2018.00015.

[61] M. Vogel, P.F. Bayi, M.T. Ruf, M.W. Bratschi, M. Bolz, A. Um Boock, M. Zwahlen, G. Pluschke, T. Junghanss, Local heat application for the treatment of Buruli ulcer: results of a phase II open label single center non comparative clinical trial, Clin. Infect. Dis. 62 (3) (2016) 342–350, https://doi.org/10.1093/cid/civ883.

[62] T. Junghanss. Thermotherapy of buruli ulcer, in: G. Pluschke. K. Röltgen (Eds.) Buruli Ulcer: Mycobacterium Ulcerans Disease, Cham (CH): Springer, 2019, 221-226.

[63] Y. Gong, Y. Wang, N. Lin, R. Wang, M. Wang, X. Zhang, Iron-based materials for simultaneous removal of heavy metal(loid)s and emerging organic contaminants from the aquatic environment: Recent advances and perspectives, Environ. Pollut. 299 (2022), https://doi.org/10.1016/j.envpol.2022.118871 118871.

[64] B.C. Hodges, E.L. Cates, J.H. Kim, Challenges and prospects of advanced oxidation water treatment processes using catalytic nanomaterials, Nature Nanotech. 13 (8) (2018) 642–650, https://doi.org/10.1038/s41565-018-0216-x.

[65] J. Yan, Y. Wang, Y. Zhang, S. Xia, J. Yu, B. Ding, Direct magnetic reinforcement of electrocatalytic ORR/OER with electromagnetic induction of magnetic catalysts, Adv. Mater. 33 (5) (2021) 2007525, https://doi.org/10.1002/adma.202007525.

[66] C.N. Hinshelwood, Kinetics of chemical change. Oxford Clarendon Press 1940.

[67] I. Langmuir, G.M.J. Mackay, The dissociation of Hydrogen into atoms. Part I. Experimental, J. Am. Chem. Soc. 36 (8) (1914) 1708–1722, https://doi.org/10.1021/ja02185a011.

[68] I. Langmuir, The dissociation of Hydrogen into atoms. Part II. Calculation of the degree of dissociation and the heat of formation, J. Am. Chem. Soc. 37 (3) (1915) 417–458, https://doi.org/10.1021/ja02168a002.

[69] W. Xu, J.S. Kong, P. Chen, Single-molecule kinetic theory of heterogeneous and enzyme catalysis, J. Phys. Chem. C. 113 (6) (2009) 2393–2404, https://doi.org/10.1021/jp808240c.

[70] K.V. Kumar, K. Porkodi, F. Rocha, Langmuir-Hinshelwood kinetics - A theoretical study, Catal. Commun. 9 (1) (2008) 82–84, https://doi.org/10.1016/j.catcom.2007.05.019.

[71] K.V. Kumar, K. Porkodi, A. Selvaganapathi, Constrain in solving Langmuir-Hinshelwood kinetic expression for the photocatalytic degradation of Auramine O aqueous solutions by ZnO catalyst, Dyes Pigm. 75 (1) (2007) 246–249, https://doi.org/10.1016/j.dyepig.2006.05.035.

[72] A. Ritter, R. Muñoz-Carpena, Performance evaluation of hydrological models: Statistical significance for reducing subjectivity in goodness-of-fit assessments, J. Hydrol. 480 (2013) 33–45, https://doi.org/10.1016/j.jhydrol.2012.12.004.

[73] F.L. Rivera, F.J. Recio, F.J. Palomares, J. Sánchez-Marcos, N. Menéndez, E. Mazarío, P. Herrasti, Fenton-like degradation enhancement of methylene blue dye with magnetic heating induction, J. Electroanal. Chem. 879 (2020), https://doi.org/10.1016/j.jelechem.2020.114773 114773.